

Proceedings of the ASME 2019 14th International Manufacturing Science and Engineering Conference MSEC2019

June 10-14, 2019, Erie, PA, USA

MSEC2019-2844

MODELING FOR CHEMICAL-ETCHING ENHANCED PULSED LASER ABLATION

Xing Zhang, Bo Mao, Rebecca Histed, Yiliang Liao*

Department of Mechanical Engineering, University of Nevada, Reno, Reno, NV 89557 Corresponding author email: yliao@unr.edu

ABSTRACT

Pulsed laser ablation (PLA) under active liquid confinement, also known as chemical etching enhanced pulsed laser ablation (CE-PLA), has emerged as a novel laser processing methodology, which breaks the current major limitation in underwater PLA caused by the breakdown plasma and effectively improves the efficiencies of underwater PLA-based processes, such as laserassisted nano-/micro-machining and laser shock processing. Despite of experimental efforts, little attention has been paid on CE-PLA process modeling. In this study, an extended twotemperature model is proposed to predict the temporal/spatial evolution of the electron-lattice temperature and the ablation rate in the CE-PLA process. The model is developed with considerations on the temperature-dependent electronic thermal properties and optical properties of the target material. The ablation rate is formulated by incorporating the mutual promotion between ablation and etching processes. The simulation results are validated by the experimental data of CE-PLA of zinc under the liquid confinement of hydrogen peroxide.

INTRODUCTION

Nanosecond pulsed laser ablation (ns-PLA) under a liquid confinement has been widely applied to industrial applications, such as laser shock processing (LSP) [1], laser micromachining [2] and PLA-based synthesis of nanocrystals [3]. During the ns-PLA, the target material is instantaneously heated and ablated when a laser pulse is irradiated onto the target surface. The laser-matter interactions lead to the formation of laser-induced plasma, which tends to expand to free space. Introducing a liquid confinement like water (H₂O) will confine the hydrodynamic expansion of laser-induced plasma, resulting in the high-

temperature-high-pressure state of plasma. As a result, PLA efficiency is significantly improved due to the confining effect of liquid confinement [4].

Despite a variety of industry applications, PLA under a liquid confinement suffers from a major drawback: when the laser intensity is above a certain threshold, a secondary plasma induced by the breakdown of the liquid confinement can be generated [5-8], which screens the incident laser energy. The breakdown phenomena of liquid confinement results in a saturation of laser ablation rate, and therefore, restricts the capability and efficiency of PLA. In order to tackle the challenge of breakdown plasma-screening effect, a chemical etching enhanced pulse laser ablation (CE-PLA) approach has been developed in recent years [9-11]. By applying an active liquid confinement such as acetic acid or hydrogen peroxide (H₂O₂), the efficiency of PLA is significantly enhanced due to the mutual promotion between the laser ablation and localized ultrafast chemical etching. For instance, Liao et al. [9] conducted experiments of ns-PLA of aluminum alloy 6061 (AA6061) and zinc (Zn) under the liquid confinement of H₂O₂. It was reported that as compared to conventional PLA under H₂O, PLA of Zn under H₂O₂ resulted in a dramatic increase of laser ablation rate.

Despite these experimental studies, few research efforts have been put on CE-PLA process modeling. In order to advance the fundamental understanding of CE-PLA and enable its industry applications, in this paper, an extended two-temperature model is proposed to predict the temporal/spatial evolution of the electron-lattice temperature and the ablation rate in the CE-PLA process. The model is developed with considerations on the temperature-dependent electronic thermal properties and the optical properties of the target material. The ablation rate is formulated by incorporating the mutual promotion between ablation and etching processes. The ablation profile and ablation depth are simulated and compared with experimental data of CE-

PLA of Zn under the liquid confinement of H₂O₂.

EXPERIMENT

Zn ingot with a diameter of 25 mm and a height of 17 mm was used in this work. Prior to CE-PLA, the samples were ground using SiC sandpaper (up to 1200 grit), followed by ultrasonic cleaning in ethanol solution. Afterwards, the samples were immersed in a beaker with H₂O₂ (30% aq.) solution resulting in about 5-mm-thick liquid layer over the ingot. CE-PLA experiments was then carried out using a Surelite III Q-switched Nd-YAG laser with a wavelength of 1064 nm and a pulse width of 5 ns. The characterization of the ablated region was conducted using an R-Tech Muti-Functional Tribometer.

MODEL DESCRIPTION

Two-temperature Model

The energy transport among the incident laser pulse, electrons and lattice can be described using the three-dimensional (3D) two-temperature thermal diffusion model, in which the spatial and temporal evolutions of the electrons and phonons distributions can be characterized in terms of electron temperature T_e and lattice temperature T_l [12]:

$$C_{e} \frac{\partial T_{e}}{\partial t} = \nabla \cdot (k_{e} \nabla T_{e}) - \Gamma_{ep} (T_{e} - T_{l}) + S, \tag{1}$$

$$C_{l} \frac{\partial T_{l}}{\partial t} = \nabla \cdot (k_{l} \nabla T_{l}) + \Gamma_{ep} (T_{e} - T_{l}), \qquad (2)$$

where C_e and C_l are the volumetric heat capacities of the electrons and lattice, respectively. k_e and k_l are the denotes of the thermal conductivities for the electrons and lattice, respectively. t is the time from the initiation of the pulse, S is the source term representing thermal input and Γ_{ep} is the electron-phonon coupling coefficient. In the case of the ns-PLA, the equations (1) and (2) can be reduced to:

$$C_{l} \frac{\partial T}{\partial t} = \frac{\partial}{\partial z} (k_{e} \frac{\partial T}{\partial z}) + S.$$
 (3)

The temperature-dependent electron and lattice heat capacities can be calculated as [13, 14]:

$$C_{e}(T_{e}) = \frac{\pi^{2} n_{e} k_{B}^{2}}{2\varepsilon_{F}} T_{e}, \ C_{l}(T_{l}) = 9N k_{B} \left(\frac{T_{l}}{T_{D}}\right)^{3} \int_{0}^{x_{D}} dx \frac{x^{4} e^{x}}{\left(e^{x} - 1\right)^{2}}, \ (4)$$

respectively, where n_e is the density of free electrons, k_B is the Boltzmann constant, ε_F is the electron Fermi energy and T_D is the Debye temperature. x and x_D can be determined by $x = \hbar \omega / k_B T_I$ and $x_D = T_D/T_I$, where ω is the angular frequency The general form of the electron thermal conductivity can be written based on the Drude model [15]:

$$k_e = \frac{1}{3} v^2 \tau C_e(T_e),$$
 (5)

where v is the electron speed, which can be taken as the Fermi velocity v_F , as only the electrons close to Fermi level contribute to the thermal conductivity. Since the electron thermal relaxation time τ is contributed from both electron-electron and electron-phonon scatterings, the total electron scattering rate $1/\tau$ can be

written as the sum of the electron-electron scattering rate and electron-phonon scattering rate, $I/\tau = I/\tau_{e-e} + I/\tau_{e-p}$, where $I/\tau_{e-e} = AT_e^2$ and $I/\tau_{e-p} = BT_l$. A and B are material constants with typical magnitude scales of $A \sim 10^7 \text{ s}^{-1}\text{K}^{-2}$ and $B \sim 10^{11} \text{ s}^{-1}\text{K}^{-2}$ for metals, and can be calculated by [16]:

$$A = \frac{\pi^2 n_e k_B^2}{3m^*} \frac{W_{e-e}}{T},\tag{6}$$

$$B = \frac{n_e e^2}{m * T} \frac{Q}{T},\tag{7}$$

where W_{e-e}/T is the thermal resistivity's linear dependence on temperature, e is the electron charge, and m^* is the effective mass of the electron. Q/T is the electrical resistivity's linear dependence on temperature obtained by fitting the data at a low temperature.

Mechanism of Material Removal during CE-PLA

To understand the mechanism of material removal during the CE-PLA process, a schematic is shown as Fig. 1. When the laser beam is irradiated onto the target surface, the target material is heated and evaporated. The laser-induced plasma plume with extremely high temperature provides an ideal environment for the decomposition reaction of H₂O₂, releasing the atomic oxygen as a strong oxidizer for the chemical etching process. Moreover, a certain amount of the released atomic oxygen could be further ionized by absorbing the later laser energy to form the ionized oxygen (O⁺) as a stronger oxidizer due to the inverse bremsstrahlung process. Consequently, the high concentration of atomic and ionized oxygen lead to an ultrafast chemical etching induced material removal, resulting in the increase of plasma density and thus the pressure and temperature. On the other hand, the etching-induced enhancement of plasma temperature and pressure can promote the ablation efficiency due to the localized confining effect attributed to the liquid confinement. In addition, the thermal energy ΔE_T released by the etching reaction could contribute to a further increase of plasma temperature. Therefore, there exists a mutual promotion relationship between the laser ablation and chemical etching processes.

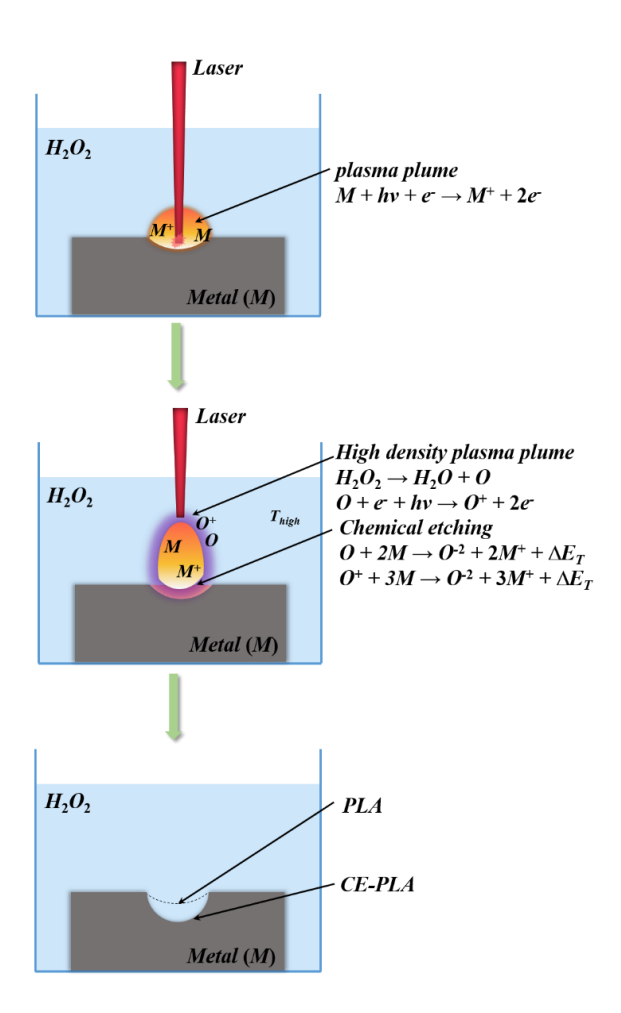


Figure 1. The schematic illustration of the CE-PLA process.

Laser Ablation-induced Material Removal

When the laser fluence exceeds the ablation criterion, $F > F_{th}$ (corresponding to critical laser intensity $I_{th} = 0.28$ GW/cm² for PLA of Zn), the ablation-induced recession of the irradiated surface can be calculated by the Hertz-Knudsen equation [17]:

$$v_a = c_s \frac{\sqrt{M}}{\sqrt{2\pi k_B T_s}} \frac{p_s}{\rho},\tag{8}$$

where v_a is the recession velocity of the irradiated surface due to the evaporation process, M is the atomic mass of the target material, and k_B is the Boltzmann constant. T_s is the surface temperature, and can be replaced by the electron/lattice temperature, $T_s = T_e = T_l$. c_s is the sticking coefficient with accounting for the back-flux of the ablated material. p_s is the saturated vapor pressure as given by the Clausius-Clapeyron equation [17]:

$$p_{s} = p_{0} Exp[\frac{MH_{v}(T_{b})}{k_{B}}(\frac{1}{T_{b}} - \frac{1}{T_{s}})],$$
 (9)

where $H_v(T_b)$ is the latent heat of vaporization at the normal boiling point T_b , and p_0 =1.013 × 10⁵ Pa is the standard atmospheric pressure. The ablation depth h_{vap} corresponding to a

single pulse can be computed by the time integration of the recession velocity [18]:

$$h_{vap} = \int_0^{\tau_I} v_a dt, \tag{10}$$

where τ_l is the thermal relaxation time at a temperature higher than T_b . τ_l is much longer than the pulse duration τ_L .

To calculate the ablation depth h_{vap} , the two-temperature model is integrated with Eq. (3) by setting the boundary conditions as:

$$-k\frac{\partial T}{\partial z}\Big|_{z=0} = -\rho v_a H_v(T_b) - h(T_s - T_{amb}), \ \frac{\partial T}{\partial z}\Big|_{z=L} = 0, \ (11)$$

where h is the convective coefficient of H_2O_2 , and T_{amb} is the ambient temperature which equals to the initial condition of temperature T(z, t = 0) = 300 K.

Etching-induced Material Removal

In this study, due to the existence of the active liquid environment, we consider that the plasma is confined and its expansion is insignificant within tens of ns. Thus, it is assumed that the decomposition of H_2O_2 contributing to chemical etching mostly occurs within the crater, where the high-temperature vapor/plasma plume is generated due to the laser-induced heating effect. As reported by Hong et al. [19], the decomposition rate of H_2O_2 at a high temperature (higher than 1000 K), k_r , can reach the order of magnitude of $10^8 \text{ cm}^3 \text{mol}^{-1} \text{s}^{-1}$. Therefore, the chemical-participated volume V(t) related to the high reaction rate within the ablated area can be given as:

$$V(t) = \int_0^{\tau_{II}} \int_0^{h_{vap}} \pi r^2 c_r k_r dz_{vap} dt, \qquad (12)$$

where τ_{II} is the thermal relaxation time at temperature higher than 1000 K, c_r is the concentration of H_2O_2 , and $z_{vap} = h_{vap}exp(-2r^2/w^2)$ represents that the profile of the laser ablation region is in a Gaussian shape. For the total ablation profile integrating contributions from laser ablation and etching, a relationship can be given as, $z_m = h_m exp(-2r^2/w^2)$, where $h_m = h_{vap} + h_c$ is the maximum ablation depth, h_{vap} and h_c are the evaporation depth and etching depth, respectively. h_m can be solved from the following integral-equation describing the chemical reaction-consumed volume,

$$\int_{0}^{\tau_{II}} \int_{0}^{h_{vup}} \pi r^{2} c_{r} k_{r} dz_{vup} dt = \int_{0}^{h_{m}} \pi r^{2} dz_{m} - \int_{0}^{h_{vup}} \pi r^{2} dz_{vup}.$$
(13)

Extended Thermal Model

According to the aforementioned mechanism of CE-PLA, the source term *S* representing thermal input in Eq.(4) can be given as:

$$S = I_{eff} + \Delta E_T, \tag{14}$$

where the decomposition-released thermal energy ΔE_T can be calculated by $\Delta E_T = V(t)E_{\nu}$, and E_{ν} is the volumetric thermal energy released by the chemical reaction. I_{eff} is the effective laser energy taking into account the reflectivity of target material, transmissivity of confining medium and penetration depth of the laser beam into the target material. It can be expressed as [15]:

$$I_{eff} = \alpha (1 - R) A_c I(t) e^{-\alpha z}, \qquad (15)$$

where z is the depth measured perpendicular to the target surface. A_c is the transmissivity of the confining medium to the laser. The optical properties, reflectivity R and absorption coefficient α , can be calculated by the Fresnel equation [20]:

$$R = \frac{(n-1)^2 + k^2}{(n+1)^2 + k^2}, \ \alpha = \frac{4\pi k}{\lambda}, \tag{16}$$

where n is the normal refractive index, k is the extinction coefficient and λ is the wavelength of the laser. I(t) is the temporal distribution of laser intensity for a Gaussian beam pulse and can be expressed as [21]:

$$I(t) = \frac{2}{\sqrt{\pi / \ln 2}} I_{PLA} Exp[-\frac{(t - \mu_d)^2}{2\sigma^2}],$$
 (17)

where μ_d is the delay time and σ is the pulse standard deviation, which is related to τ_L in terms of $\tau_L = 2\sqrt{2\ln 2}\sigma$. The laser intensity I_{PLA} stands for the laser energy required for the normal ns-PLA to reach the same ablation depth as CE-PLA processing with an intensity of $I_{CE-PLA} = F_{CE-PLA}/\tau_L$, where F_{CE-PLA} is the corresponding laser fluences in J/cm². The required laser intensity can be expressed as:

$$I_{PLA} = I_{CE-PLA} + \eta I_{eqv}, \qquad (18)$$

where I_{eqv} represents the equivalent laser energy by converting the etching depth into evaporation depth, and η is the CE-PLA coefficient.

Modeling Parameters

The data used to calculate the optical and thermal properties of material are listed in Table 1. The released volumetric energy E_v during chemical reaction is taken as 31.9 kJ/cm³.

Table 1. Data used to calculate the optical and thermal properties of Zn.

n	2.88
k	3.48
R	0.575
$\alpha (\mathrm{m}^{-1})$	4.1×10 ⁷
A_c	83%
m^*/m_e	0.85
$n_e (\mathrm{m}^{-3})$	1.31×10 ²⁹
W_{e-e}/T (m/W)	0.42×10 ⁻⁷
$Q/T (\Omega m/K)$	1.9×10 ⁻¹⁰
$v_F(m/s)$	1.82×10 ⁶
$\varepsilon_F(eV)$	9.39
A (s ⁻¹ K ⁻²)	0.38×10 ⁷
B (s ⁻¹ K ⁻²)	8.2×10 ¹¹

The evaporation depth h_{vap} and the etching depth h_c as affected by laser intensity can be obtained by Eqs. (10) and (13), as shown in Fig. 2. According to the calculated depth, the equivalent laser intensity I_{eqv} and the laser intensity required for underwater PLA I_{PLA} corresponding to the actual injected laser intensity I_{CE-PLA} is illustrated in Fig. 2b, where the CE-PLA

coefficient η can be deduced.

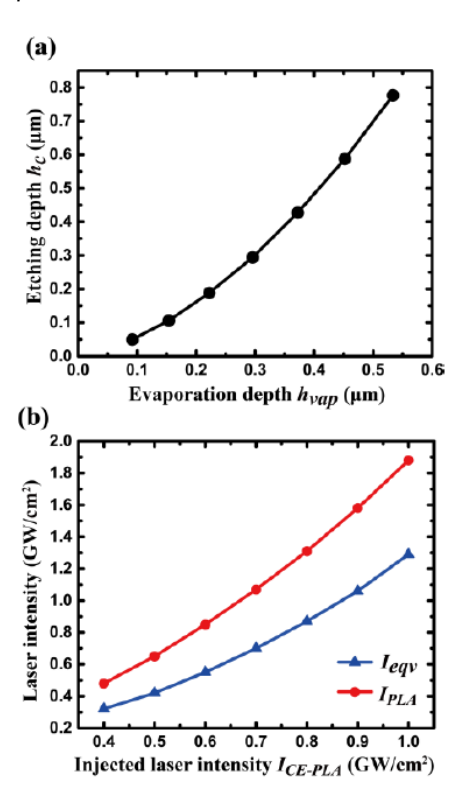


Figure 2. (a) Evaporation depth h_{vap} and the corresponding chemical etching depth h_c ; (b) The actual injected laser intensity I_{CE-PLA} with the corresponding equivalent laser intensity I_{eqv} and the laser intensity required for underwater PLA I_{PLA} .

RESULTS AND DISCUSSION

Figure 3a and 3b show the contour plots of the temperature evolution with depth and time during CE-PLA processing of Zn with an average pulse intensity of 0.64 GW/cm². colored regions depict higher temperatures in comparison to the blue colored regions, and the black curves represent equaltemperature lines. Figure 3b illustrates the temperature distribution from 8 to 30 ns and a depth from the surface to 2 µm. It is found that when the pulse is injected onto the target material, the surface temperature instantaneously increases to above 4500 K within 5 ns. According to the ablation criteria, such a high temperature leads to an instantaneously evaporative ablation of the surface layer. Subsequently, the temperature starts to decrease with a slow rate. Since the boiling point of the target material (Zn) is ~1180K, according to the Hertz-Knudsen equation, the evaporative ablation depth can be estimated from the surface temperature history. Due to the optical penetration depth, the peak temperature region (> 4500 K) is only found near the surface within a depth of tens nanometers. An apparent shift of the peaks of temperature is also observed. Figure 3b shows the tail part of the temperature evolution with the time from 30 to 150 ns and a depth of 10 µm from the surface, which

indicates that the thermal relaxation time is much longer than the pulse duration. It is clear from this figure that the temperature is kept above 1000 K for \sim 100 ns, which provides a steady environment for the ultrafast chemical reaction. In addition, as the time evolves, due to the thermal conduction, the energy is transferred from the surface to underneath, leading to an elevated temperature found up to almost 8 μm depth from the surface.

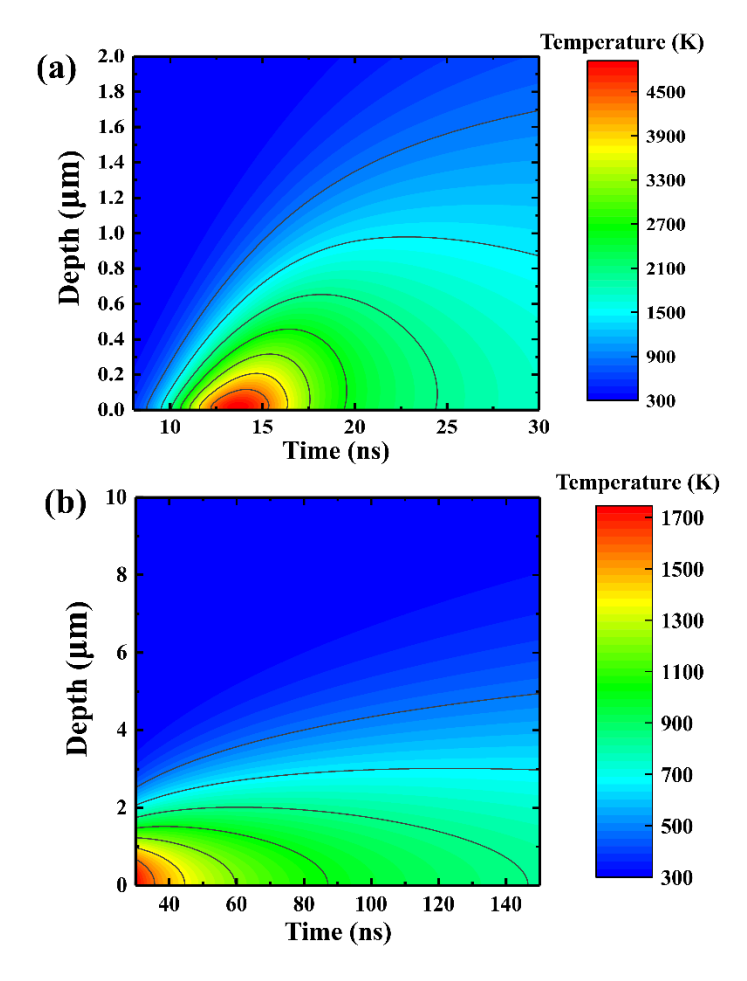


Figure 3. Simulated temporal and spatial evolutions of temperature during CE-PLA processing of Zn: (a) 0-30 ns; (b) 30-100 ns.

The experimental measurements and simulation results of the cross-section profiles of the ablated region after PLA under different confining media are shown in Fig. 4 Each profile is acquired using five laser pulses in the intensity of 0.64 GW/cm² to minimize the error introduced by the pulse energy variance. Experimental data indicate that the maximum depth at the center of the ablated region is increased by 100 % from 1.2 to 2.4 μm when utilizing H_2O_2 as the confining media instead of H_2O . Moreover, the ablation diameter at the target surface is increased by almost 10% from 1.1 to 1.2 mm. For CE-PLA under H_2O_2 confinement, the relatively long thermal relaxation period, the increased plasma density and the released energy from chemical etching result in the ablation environment at a high temperature for the ultrafast chemical reaction, leading to a significant

increase of ablation efficiency. The simulation results present a similar enhancement of ablation efficiency in CE-PLA under $\rm H_2O_2$ as compared to PLA under $\rm H_2O$. By taking into account the energy distribution in a transverse plane following the Gaussian shape, the ablated profile is obtained based on the calculated depth. It is predicted that the maximum depth is increased from 1.26 μm to 2.57 μm . The modeling results show a good agreement with experimental data, which confirms the model's capability of obtaining an ablation profile for the CE-PLA process.

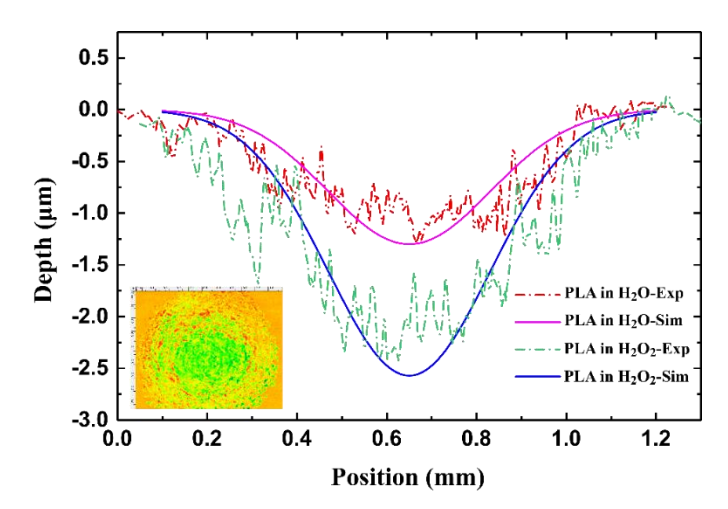
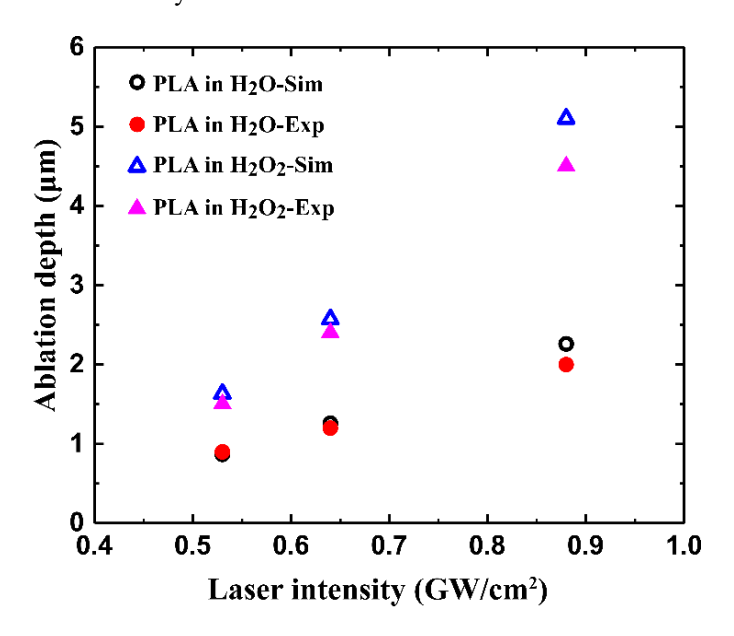


Figure 4 Comparison between experimental data and modeling results of cross-section profiles of Zn processed by PLA under H₂O and H₂O₂, five laser pulses with the laser intensity of 0.64 GW/cm².

For further model validation, a series of PLA experiments were carried out under H₂O and H₂O₂. Figure 5 illustrates the experimental and simulation results of PLA processing with five laser pulses and laser intensities of 0.53, 0.64 and 0.88 GW/cm². By comparing the experimental results under H₂O₂ and H₂O, it is found that the maximum depth at the center of the ablated region is increased at all laser intensities, such as from 0.9 to 1.5 μm at 0.53 GW/cm², and 2 to 4.5 μm at 0.88 GW/cm². Moreover, it is found that this enhancement of ablation rate becomes more significant with the increase of laser intensity. For instance, the ablation depth is improved by 67 % at 0.53 GW/cm², 100 % at 0.64 GW/cm², and 125 % at 0.88 GW/cm². This could be attributed to the fact that with the increase of laser intensity, the laser ablation region is enlarged and the thermal relaxation time is prolonged, resulting in a greater amount of H₂O₂ participating in the etching reaction. Furthermore, it is found that the strategy of applying H₂O₂ as the confinement instead of H₂O results in a much higher efficiency for enhancing the ablation rate as increasing the laser intensity. For example, by increasing the laser intensity from 0.53 to 0.64 GW/cm², PLA under H₂O and H₂O₂ result in the improvements of ablation depth by 33% and 60%, respectively. Moreover, it is demonstrated in Fig. 5 that the modeling result is consistent with the trend observed from the experimental data. The extended two-temperature based model provides accurate predictions of

the ablation profiles for laser processing with relatively low laser intensities of 0.53 and 0.64 GW/cm². For laser processing with a high intensity of 0.88 GW/cm², the small discrepancy between experimental findings and simulated data is observed. This might be attributed to the plasma screening effect, which becomes nonnegligible at a high laser intensity due to the high plasma density. The plasma-laser interaction in experiments could screen a portion of incident laser energy, and therefore lead to a lower ablation efficiency. It was reported that the plasma screening in PLA of Al starts to appear at a laser intensity of 0.8 GW/cm² [22]. However, the discrepancy is only of the order of 13% (simulated result of 5.1 µm as compared to experimental data of 4.5 µm). Overall speaking, one can conclude that the modeling results match well with the experimental findings. Future work will be directed to include the influence of plasma-laser interaction into the current model, in order to improve the accuracy and extend the universality of the laser-material interaction model.



 $\label{eq:Figure 5. Comparison of experimental results and simulation data: ablation depths (five pulses) of PLA processing of Zn under $$H_2O_2$ and H_2O as affected by laser intensity.$

CONCLUSIONS

In this paper, an extended two-temperature model is developed to predict the temporal/spatial evolution of the electron-lattice temperature and the ablation rate in the CE-PLA process. The ablation rate is formulated by incorporating the mutual promotion between ablation and etching processes. The ablation profile and ablation depth are simulated and compared with experimental data of CE-PLA of Zn under liquid confinements of H₂O₂ and H₂O. The simulation results agree well with the experimental measurements, showing that CE-PLA greatly improves the ablation efficiency of underwater ns-PLA. It can be expected that the choice of the active confinement media could be extensively applied in ways such as improving the working efficiency in laser micromachining, enhancing the

laser shock pressure in laser shock peening, increasing the productivity in PLA-based nanocrystal synthesis, etc.

ACKNOWLEDGEMENTS

The authors gratefully thank support from the U. S. National Science Foundation (NSF) (CMMI-1825739).

REFERENCES

- [1] Mao, B., Liao, Y., and Li, B., 2018, "Gradient twinning microstructure generated by laser shock peening in an AZ31B magnesium alloy," Applied Surface Science.
- [2] Mao, B., Siddaiah, A., Menezes, P. L., and Liao, Y., 2018, "Surface texturing by indirect laser shock surface patterning for manipulated friction coefficient," Journal of Materials Processing Technology, 257, pp. 227-233.
- [3] Pyatenko, A., Shimokawa, K., Yamaguchi, M., Nishimura, O., and Suzuki, M., 2004, "Synthesis of silver nanoparticles by laser ablation in pure water," Applied Physics A, 79(4-6), pp. 803-806
- [4] Yang, G., 2007, "Laser ablation in liquids: applications in the synthesis of nanocrystals," Progress in Materials Science, 52(4), pp. 648-698.
- [5] Sollier, A., Berthe, L., Peyre, P., Bartnicki, E., and Fabbro, R., "Laser-matter interaction in laser shock processing," Proc. First International Symposium on High-Power Laser Macroprocessing, International Society for Optics and Photonics, pp. 463-468.
- [6] Wu, B., and Shin, Y. C., 2006, "Laser pulse transmission through the water breakdown plasma in laser shock peening," Applied physics letters, 88(4), p. 041116.
- [7] Berthe, L., Fabbro, R., Peyre, P., and Bartnicki, E., 1998, "Experimental study of the transmission of breakdown plasma generated during laser shock processing," The European Physical Journal-Applied Physics, 3(2), pp. 215-218.
- [8] Berthe, L., Fabbro, R., Peyre, P., and Bartnicki, E., 1999, "Wavelength dependent of laser shock-wave generation in the water-confinement regime," Journal of applied physics, 85(11), pp. 7552-7555.
- [9] Liao, Y., Yang, Y., and Cheng, G. J., 2012, "Enhanced laser shock by an active liquid confinement—hydrogen peroxide," Journal of Manufacturing Science and Engineering, 134(3), p. 034503.
- [10] Hong, M., Ng, K., Xie, Q., Shi, L., and Chong, T., 2008, "Pulsed laser ablation in a cooled liquid environment," Applied Physics A, 93(1), pp. 153-157.
- [11] Luo, F., Guan, Y., Ong, W., Du, Z., Ho, G., Li, F., Sun, S., Lim, G., and Hong, M., 2014, "Enhancement of pulsed laser ablation in environmentally friendly liquid," Optics express, 22(20), pp. 23875-23882.
- [12] Vatsya, S. R., and Virk, K. S., 2003, "Solution of two-temperature thermal diffusion model of laser-metal interactions," Journal of Laser Applications, 15(4), pp. 273-278.

- [13] Jiang, L., and Tsai, H.-L., 2005, "Improved two-temperature model and its application in ultrashort laser heating of metal films," Journal of heat transfer, 127(10), pp. 1167-1173.
- [14] Balaguru, R. J. B., and Jeyaprakash, B., 2015, "Lattice Vibrations, Phonons, Specific Heat Capacity, Thermal Conductivity."
- [15] Ivanov, D. S., and Zhigilei, L. V., 2003, "Combined atomistic-continuum modeling of short-pulse laser melting and disintegration of metal films," Physical Review B, 68(6), p. 064114.
- [16] Vestentoft, K., and Balling, P., 2006, "Formation of an extended nanostructured metal surface by ultra-short laser pulses: single-pulse ablation in the high-fluence limit," Applied Physics A, 84(1-2), pp. 207-213.
- [17] Lutey, A. H., 2013, "An improved model for nanosecond pulsed laser ablation of metals," Journal of Applied Physics, 114(8), p. 083108.
- [18] Mihai State, A. M., Niculae N. Puscas, 2014, "Pulsed Laser Ablation of Solids, Basics, Theory and Applications."
- [19] Hong, Z. K., Farooq, A., Barbour, E. A., Davidson, D. F., and Hanson, R. K., 2009, "Hydrogen Peroxide Decomposition Rate: A Shock Tube Study Using Tunable Laser Absorption of H2O near 2.5 mu m," J Phys Chem A, 113(46), pp. 12919-12925.
- [20] Winter, J., Rapp, S., Schmidt, M., and Huber, H. P., 2017, "Ultrafast laser processing of copper: A comparative study of experimental and simulated transient optical properties," Applied Surface Science, 417, pp. 2-15.
- [21] Hatef, A., Fortin-Deschênes, S., and Meunier, M., "Simulation of nanosecond laser-induced thermal dynamics of hollow gold nanoshells for hyperthermia therapy," Proc. AIP Conference Proceedings, AIP, pp. 105-110.
- [22] Zhang, Y., Zhang, D., Wu, J., He, Z., and Deng, X., 2017, "A thermal model for nanosecond pulsed laser ablation of aluminum," AIP Advances, 7(7), p. 075010.